

Automated Classification of 2000 Bright IRAS Sources

Ranjan Gupta

IUCAA, Post Bag 4, Ganeshkhind, Pune-411007, India

rag@iucaa.ernet.in

Harinder P. Singh

Department of Physics & Astrophysics, University of Delhi, Delhi-110007, India

hpsingh@physics.du.ac.in

K. Volk and S. Kwok

*Department of Physics & Astronomy, University of Calgary, 500 University Dr.,
N.W., Calgary, Alberta, Canada T2N 1N4*

volk@iras.ucalgary.ca ; kwok@iras.ucalgary.ca

ABSTRACT

An Artificial Neural Network (ANN) scheme has been employed that uses a supervised back-propagation algorithm to classify 2000 bright sources from the Calgary database of IRAS (Infrared Astronomical Satellite) spectra in the region $8\mu\text{m}$ to $23\mu\text{m}$. The database has been classified into 17 predefined classes based on the spectral morphology. We have been able to classify over 80 percent of the sources correctly in the first instance. The speed and robustness of the scheme will allow us to classify the whole of the LRS database, containing more than 50,000 sources, in the near future.

Subject headings: infrared: galaxies — methods: data analysis

1. Introduction

Infrared Astronomical Satellite Low Resolution Spectrometer (LRS) recorded spectra of some 50,000 sources in blue ($8 - 15\mu\text{m}$) with $\lambda/\Delta\lambda \sim 40$ and in red ($13 - 23\mu\text{m}$) with a resolution ~ 20 . A total of 5425 objects with better quality spectra were included in the Atlas of low-resolution IRAS spectra (1986, hereafter the Atlas). Volk & Cohen (1989a)

published spectra of 356 IRAS point sources with $F_{\nu}(12\mu\text{m}) > 40\text{Jy}$ that were not included in the Atlas. These brighter sources were classified into nine classes based upon the spectral morphology. Sixty percent of the sources have silicate emission and red-continuum spectra associated with H II region sources. No emission-line sources formed part of the set of 356 spectra. This sample was also used to test the classification scheme of IRAS sources based on broad-band colors. Classifiable spectra were found for 338 of the sources in the sample. The remaining 18 sources had either extremely noisy or incomplete spectra. It was found that some class of sources overlapped on the color-color diagrams and, therefore, the nature of some of the IRAS sources could not be determined from the IRAS photometry.

Volk et al. (1991) published an additional 486 spectra belonging to sources with $12\mu\text{m}$ fluxes between 20 and 40Jy that were also not in the Atlas. Classifiable spectra were found for 424 sources. The spectra were classified into nine groups as in Volk & Cohen (1989a) that describe the astrophysical nature of these sources. Kwok, Volk & Bidelman (1997) processed 11,224 spectra (including sources in the Atlas), corresponding to a flux limit of 7Jy at $12\mu\text{m}$. These spectra were also classified by-eye and put into nine classes based on the presence of emission and absorption features and on the shape of the continuum. They identified optical counterparts of these IRAS sources in the existing optical and infrared catalogs and listed the optical spectral types if they were known.

It is evident that large databases like the one referred to above require automated schemes for any analysis. Artificial Neural Networks (ANN) have been employed extensively in several branches of Astronomy for automated data analysis (Lahav & Storrie-Lombardi, 1994). ANN have been used previously by the IUCAA group in three distinct areas of stellar Astronomy. They have been applied to classify digitized optical and ultraviolet spectra (Gulati et al. 1994a,b; Singh et al. 1998); to compare a set of observed spectra of F & G dwarfs with a library of synthetic spectra (Gulati et al. 1997a, Gupta et al. 2001); and to determine the reddening properties of hot stars from the low-dispersion ultraviolet spectra (Gulati et al. 1997b).

We have attempted to classify 2000 brightest sources from the Atlas into 17 classes by means of Artificial Neural Networks. In the next section we describe features of the 17 new classes. In Section 3, we present details of the ANN scheme. Results are discussed in Section 4 and important conclusions of the study are presented in the last section. Further, an appendix has been added just before the reference section, to explain the general ANN architecture for the benefit of the readers.

2. Spectral Classes

The set of 2000 spectra were classified into the 17 classes by-eye by one of us (K. Volk). These classifications are assumed to form the reference set of “correct” classifications. Such by-eye classification has an element of subjectivity in it, and is more apt to have problems when the spectra are noisy. This set of 2000 sources are the brightest sources in the LRS atlas and have the least problems with noise or spectral peculiarities. This makes the by-eye classification as accurate as possible despite the element of subjectivity.

The groups used for spectral classification are an extension of the nine classes described in Volk & Cohen (1989a). The current scheme introduces more classes, for three reasons:

(a) The “HII region sources” group shows a variety of features, and so separate classes have been made for the more obvious feature types so that these classes are, one hopes, more uniform;

(b) A few new classes have been created within the $10\ \mu\text{m}$ silicate feature and $11.3\ \mu\text{m}$ SiC feature groups to divide the objects with weaker features from those with stronger features; and

(c) Some small groups of unusual sources can be identified from the “usual/unknown” group of Volk & Cohen (1989a), hence these were given their own classes here such as class 14 for $21\ \mu\text{m}$ feature sources.

The division between the spectra with “stronger” and “weaker” features was made at LRS type 25 or 45 (for silicate emission sources and SiC emission feature sources respectively) since the original LRS classes are based upon the feature strength. Thus the spectra with strong features, LRS types 25 to 29 or 45 to 49, are separated from the spectra with weaker features, LRS types 21 to 24 or 41 to 44. All objects with LRS classes near the dividing line were examined by-eye to make sure that the LRS type accurately reflects the feature strength. In some cases this led to spectra being placed into the “stronger” or “weaker” feature groups even when the LRS type is not as expected. In the large majority of cases no problem with the LRS type was found.

A short summary of the 17 classes is given in Table 1, with representative spectra plotted in Figure 1. A detailed description of the different classes and their relation to the original LRS types now follows:

(0) Line emission sources

This class is for spectra with strong emission lines (line peak to continuum ratio of 1 or larger) and no obvious dust emission or absorption features. These are nearly all planetary nebula sources. A few cases of HII region sources that may show the $12.8 \mu\text{m}$ [NeII] line could have been included here, but were left in the other “HII region” groups since the $12.8 \mu\text{m}$ emission line seen in LRS spectra is sometime due to an instrumental problem rather than being an actual emission line, and since the possible [NeII] lines were relatively weak. Comparatively few HII region spectra have strong enough emission lines as observed by the LRS instrument to be potentially included in this group. In the original LRS classification, these are generally classified as types 81 to 96.

The prototype spectrum in Figure 1 shows several emission lines: $9.0 \mu\text{m}$ [ArIII], $12.8 \mu\text{m}$ [NeII], $15.5 \mu\text{m}$ [NeV], and $18.7 \mu\text{m}$ [SIII]. Other objects in this class tend to have fewer emission lines than this example.

(1) Sources with stronger $11.3 \mu\text{m}$ SiC emission features

In this group one has evolved carbon stars undergoing mass loss and showing a strong $11.3 \mu\text{m}$ emission feature. In the original LRS classification these would be type 45 to 49 sources, implying the feature peak to estimated continuum ratio is larger than 1.648.

(2) Stellar continuum sources

Here is the class for stars without circumstellar dust shells that radiate significantly in the 8 to $23 \mu\text{m}$ region, including Vega, Sirius, Aldebaran, and Antares. Most of these sources are of K-type to early M-type. Only a few have spectral types earlier than K0. In the original LRS classification these would be type 16 to 19 sources

(3) Featureless sources with cooler colour temperatures

This group is as in Volk & Cohen (1989a). The continuum colour temperature is lower than expected for the photospheric emission of any normal star, including late M-type stars. Aside from the unusually low colour temperature for a stellar photosphere there is no overt sign of any dust emission. Many of these sources have optical counterparts among known Mira or irregular variables of M-type. In the original LRS classification these would be type

12 to 15 sources. All featureless continuum sources with λF_λ ratios of less than 3 between 7.9 and 11 μm but which still have declining continua over the LRS wavelength range are placed in this class.

(4) Sources with UIR features at 7.6/8.5/11.3/12.5 μm

This group includes sources with the UIR features, except for those with very steep (“red” according to the LRS atlas definition) continua which form class 16. These would ideally be type 80 sources in the original LRS classification, but there was considerable confusion with other types of objects.

As long as the spectrum signal to noise ratio is reasonable it is possible to objectively distinguish between UIR feature spectra and silicate absorption, as discussed in Volk & Cohen (1989b).

(5) Sources with 10 μm silicate absorption

This class includes objects with silicate absorption features, but we attempt to exclude cases of compact HII regions with foreground silicate absorption which have much lower continuum colour temperature than the “normal” silicate absorption feature sources such as IRAS 01304+6211 (see Figure 1). If the spectral continuum is rising from 7.6 to 23 μm and there is a silicate absorption feature at 10 μm the spectrum is put in class 9. In the original LRS classification class 5 sources correspond to types 31 to 39. An additional refinement is that sources that are in transition between silicate emission and silicate absorption at 10 μm are grouped in class 13.

(6) Sources with strong silicate emission at 10 μm

Spectra with a falling continuum over the LRS wavelength range and having a silicate emission feature with a peak greater than 1.628 times the continuum are in this class. These would be types 25 to 29 in the original LRS classification. Similar spectra but with weaker features are put into class 12.

(7) Sources with low temperature ($\leq 100^\circ\text{K}$) dust continuum emission

In this group are mostly HII region spectra which do not show very strong features due to silicates or the UIR features. The continuum must rise over the LRS wavelength range from 7.6 to 23 μm for a spectrum to be included in this class, corresponding roughly to a colour temperature of less than 100°K, but generally the continuum shape cannot be described by a single colour temperature. In the original LRS classification these would have been given some type in the 60's, 70's, or 80's. In a few unusual cases there can be other types of spectra mixed into this group. When there are accompanying strong features such as the 10 μm feature in emission or absorption the spectra are put into classes 8, 9, or 12.

(8) Sources with silicate emission and a low temperature dust continuum

Here are spectra with continuum shape similar to that of class 7 but with a clear 10 μm silicate emission feature. In principle this corresponds to types 61 to 69 in the original LRS classification. Some of the sources are HII regions, but others are young planetary nebulae such as Hb 12, Vy 2-2, and SwSt-1; others are their immediate progenitors caught in the phase between the asymptotic giant branch phase and the planetary nebula phase (“protoplanetary nebulae” or PPNs) such as HD 161796 and IRAS 18095+2704. The spectrum of 18095+2704 is shown in Figure 1; this has unusually strong features and the continuum is not as steeply rising as is typically the case for spectra in this class.

(9) Sources with silicate emission and a low temperature dust continuum

This is another class where the continuum is required to rise over the LRS wavelength range from 7.6 to 23 μm . Here we include spectra showing the 10 and 18 μm silicate features in absorption. These are nearly all compact HII region sources with (presumably) foreground cold dust in the associate molecular cloud. In the original LRS classification these would be type 71 to 79 sources.

(10) Extreme carbon stars

The prototype for this group is AFGL 3068 (IRAS 23166+1655), which is known to be a carbon star with an extremely optically thick dust shell. The spectra are selected for this group on the basis of having low colour temperatures (of order 300°K) in the 10 μm region of the spectrum and of having no strong emission or absorption features. In some cases there is some type of weak feature around 11 μm which might be due to the 11.3 μm SiC feature in emission or weak absorption. These objects are discussed in Volk, Kwok, & Langill (1992).

(11) Low colour temperature featureless spectra

The group of spectra have low colour temperature (about 150 to 200°K) featureless continua. They have noticeably lower colour temperatures than the extreme carbon star spectra (see Figure 1) but peak somewhere in the LRS wavelength range and decline thereafter, unlike the HII region spectra in classes 7, 9, and 16. A few of these sources are known to be either young planetary nebulae or PPNs, and they all seem to have carbon-based dust shells. These objects are discussed by Volk, Kwok & Woodsworth (1993). In the original LRS classification they were generally assigned type 05 or 50.

(12) Sources with weaker silicate emission features

This group of spectra is the analogue of class 6, but they have feature peak to continuum ratios of less than 1.628. In the original LRS atlas classification these would be type 21 to 24 spectra. In various cases the feature was not detected at all in the original LRS atlas classification and these were generally classified as type 15 to 18.

(13) Sources with intermediate optical depth silicate dust shells

Prototype spectra for this class include IRAS 19192+0922, IRAS 17125–4814, IRAS 15119–6453, and IRAS 16546–4047 (see Figure 1). All these spectra have continua which fall between 7.6 and 23 μm . The optical depth of the dust shells in these objects is such that the 10 μm feature is in transition between emission and absorption while the 18 μm feature is still in emission. In the original LRS classification these were often confused with SiC emission spectra, and so given erroneous types of 41 to 45.

(14) Source with the 21 μm feature

A small number of sources are known to have a dust feature at 21 μm , one possible identification of which is TiC grains (von Helden et al., 2000). The feature was discovered in the LRS spectra. Less than 20 such sources are known, the brighter of which are used to define the group here. All sources in this group are carbon-rich PPNs. A few extreme carbon stars and the planetary nebula IC 418 appear to have very weak 21 μm features, but these require the *Infrared Space Observatory* to detect and so they are not included here.

(15) Sources with weaker 11.3 μm SiC emission

All spectra from carbon stars with the 11.3 μm feature but with a feature to continuum ratio of less and 1.628 are put in this group, which is closely analogous to class 1. In the original LRS classification these would be of type 41 to 44.

(16) Cool continuum sources with strong UIR features

Any spectrum which has a continuum that rises from 7.6 to 23 μm (allowing for the possibility of a strong 7.6 μm feature at the short wavelength end of the spectrum) and strong UIR features at 7.6 and 11.3 μm is placed in this class. These are HII region spectra with UIR features. In the original LRS classification these would be of type 80 or 81. In some cases it is possible that there is an underlying silicate absorption component as well as the UIR features, causing a very large rise at the short wavelength end of the LRS spectrum. However these spectra lack any 18 μm absorption feature which makes the presence of strong 10 μm silicate absorption less likely.

3. ANN Scheme

In this analysis, we have used the multi-layer back-propagation (MBPN) neural network scheme with supervised learning as described in Gulati et al. (1994a,b). This scheme requires a set of spectra to be predefined as the training set and should include all the classes of the unknown set that the network is supposed to classify. The algorithm trains on this training set and subsequently in the test phase, classifies the unknown test set into the predefined classes.

A training set of 170 spectra having 10 sources for each training class was set aside for training purposes. Fig. 1 shows a representative sample of each of these 17 classes. Each spectrum consists of 93 flux values in the range of 8 – 23 μm . We may mention that 148 numbers of the 170 training spectra were included in the 2000 test spectra for validity checks.

The ANN scheme involved using this set of 170 input spectra with 17 assigned classes (0 to 16) to train the ANN algorithm. We refer to these classes as the catalog classes. The ANN configuration used was 93-16-16-17, implying 93 data points for each of the 17 output spectral classes with two hidden layers of 16 nodes each (a detailed explanation on the ANN architecture is given in the Appendix). The training session involved an iterative procedure with the network weights getting modified at each iteration. During an iteration,

the computed output and the desired output were compared and the resultant error was then utilized to modify the network weights for the next iteration using a back propagation algorithm. The learning or training was stopped once the error was minimized to a predefined level and the network weights were considered to be frozen (Gulati et al. 1994a). A learning curve for 10000 iterations is given in Fig. 2 (left panel).

Subsequent to the above training session, the test session uses the frozen weights determined above to perform the classification of the 2000 test set of spectra into 17 catalog classes.

4. Results and Discussion

A general picture of the result of our ANN classification scheme is given in Fig. 2 (right panel) in the form of a histogram. A total of 1,618 spectra have been classified correctly out of the total sample of 2000 source spectra indicating a success rate of 80% at the first instance. Table 2 provides a summary of the ANN classification of the 2000 test sources into the 17 groups or classes. Table 3 lists 382 of the misclassified sources with their catalog class and the corresponding ANN class. In the following, we describe some finer details of the classification accuracy for individual classes 0 to 16.

Out of a total 23 spectra for class 0, 19 were classified correctly. From the four that were misclassified, one each was classified as class 7, 8, 13, and 16. Table 3 lists the 4 spectra of class 0 that were misclassified. Source 22036+5306 has been put in class 16 by the ANN probably because of the strong feature at around $8\mu\text{m}$, typical of class 16.

Out of a total 136 spectra for class 1, 113 were classified correctly. From the 23 that were misclassified, 11 were misclassified into class 13; 6 were misclassified into class 15, 3 were misclassified into class 4, 2 were misclassified into class 6 and 1 was misclassified into class 14. The misclassified sources of class 1 are listed in Table 3. Out of these, 18 spectra seem to belong to the class assigned by the ANN and not the catalog class, specially those put into classes 13 and 15. ANN Classification accuracy of class 2 has the best agreement with the catalog class. Out of 89 spectra of class 2, 88 spectra were classified correctly while 1 spectrum was misclassified into class 3.

Of the 94 spectra for class 3, 85 were classified correctly. Of the 9 that were misclassified, 5 were misclassified into class 2 and 1 each into classes 1, 12, 13 and 15. At least 1 source (20056+1834) has a spectrum which does not seem to belong to class 3 and has been put in class 13 by the ANN.

Of a total of 87 sources of class 4, 34 were correctly classified while 53 were misclassified; 22 into class 5, 11 into class 16, 10 into class 13, 4 into class 15, 2 each into class 9 and 14 and 1 each into class 2 and 10. As mentioned in Sec. 2, class 4 corresponds to type 80 sources in the original LRS classification in which there was a lot of confusion with the other types of sources. ANN put 22 sources into class 5, which has sources with $10\mu\text{m}$ silicate absorption feature. We note that in the training sample of class 4, there are at least two sources (16367–4701 & 19327+3024) which might be resulting in contamination of this class with class 5 and hence less than efficient training for class 4.

Out of a total of 103 spectra for class 5, 88 were correctly classified. 7 spectra were misclassified into class 16, 4 into class 4, 2 into class 9 and 1 each into class 13 and 14. ANN has correctly picked up at least 3 spectra from the catalog that should be put in class 4 (Table 3).

Class 6 (strong $10\mu\text{m}$ feature) has the largest sample of 735 sources. Out of these 679 were classified correctly and 33 were misinterpreted as class 12 (weak $10\mu\text{m}$ feature). Similarly, class 12 has 198 spectra out of which 15 were misclassified as class 6, while 27 were misclassified into class 3. As discussed later, if one were to treat a weak and a strong $10\mu\text{m}$ feature sources as belonging to a single class, percentage of correctly classified sources will be in excess of 90% for these classes.

For class 7, out of the 53 sources, 45 have been classified correctly. 3 sources were incorrectly classified into class 0 while 2 sources each were incorrectly classified into classes 9 and 11. Class 8 has 13 sources out of which only one has been wrongly classified into class 0.

Class 9 has 40 sources in all. 26 have been correctly classified, 4 each have been misclassified into classes 7 and 14 and 3 each into classes 5 and 16. Class 10 has 44 sources in all and 38 have been correctly classified but 3 have been wrongly classified to class 13, 2 into class 6 and 1 into class 1. Class 11 has 12 sources out of which 8 were correctly classified. 3 sources were incorrectly classified into class 14 and 1 into class 0.

As mentioned in Section 2, in the original LRS classification, class 13 spectra were often confused with SiC feature sources. In the ANN classification also, out of the 200 class 13 sources, 104 were wrongly classified (85 into class 6) while 96 were correctly classified. The wrongly classified sources have been listed in Table 3 for the purpose of review by the human classifiers.

Class 14 has 3 sources out of which one was misclassified into class 10. Class 15 had 140 sources out of which 111 have been correctly classified. But 18 have been classified into class 1 and 3 each into classes 13 and 4; 2 each into class 2 and 4, and 1 into class 3. Lastly,

25 sources out of a total of 30 of class 16 were classified correctly. 2 sources were wrongly classified into class 7 while 1 each were classified into classes 0, 1 and 5.

If we assume classes 6 and 12 to be the same, (class 12 trained as class 6) and redo the classification exercise, we obtain the overall classification histogram as shown in Fig. 3. A total of 1,675 spectra have now been classified correctly which is about 84% of the total test data set. This process also improved the classification of the class 6 sources which is shown in Fig. 5.

We split off class 12 from class 6 because it improved the classification of silicate emission objects. With the full range of silicate emission objects in one class there was more dispersion of values and the ANN system had more chance of misclassification. However, it does not matter that sources are misclassified from class 6 to class 12 or class 12 to class 6 because the dividing line between these two groups is not sharp and there is a continuous range of silicate feature strengths, and some objects must fall at the boundary.

Fig. 6 shows the improvement in the class 13 classification, namely earlier 85 sources of this class were wrongly classified as class 6 which has now reduced to 50 wrong classifications. This process also improved the classification of class 4 as seen in Fig. 4. There were such improvements noticed in general and Fig. 3 is really a combined effect of all these.

5. Conclusions

We have demonstrated in this paper the application of ANN scheme to a large database of 2000 IRAS spectra and have been able to correctly classify more than 80% of the data-set. The misclassified spectra were looked in detail and most of them could have been wrongly catalogued or had features which would have been confusing for even a human classifier.

We stress here that the speed and robustness of this scheme can be very useful for classifying the whole of LRS database containing over 50,000 sources.

RG and HPS are grateful to SK and KV for kind hospitality while on a visit to Calgary. We thank the two anonymous referees for very useful comments.

A. ANN architecture

In a feedforward neural network there are several inputs, a few hidden layers, and several outputs (Bailer-Jones et. al., 2002). See the Figure 7 for a block view of this architecture. Each node in the input layer holds a value, x_i . In our example application, the input vector, $(x_1, x_2, \dots, x_i, \dots)$, is the spectrum with 93 flux values, and the output vector, $(y_1, y_2, \dots, y_l, \dots)$, has 17 nodes. Each of the input nodes connects to every node in the next layer of nodes, the first ‘hidden’ layer, and each of these connections has a weight, $w_{i,j}$, associated with it. A node in the hidden layer forms a weighted sum of its inputs, and passes this through a *nonlinear transfer function*, such that the output from the j^{th} hidden node is

$$p_j = \tanh \left(\sum_i w_{i,j} x_i \right) . \quad (A.1)$$

These values are passed to a second hidden layer which performs a similar processing, the output from that layer being the vector \mathbf{q}

$$q_k = \tanh \left(\sum_j w_{j,k} p_j \right) . \quad (A.2)$$

The output layer then performs a simple sum of its inputs, so that the network output, y_l , is

$$y_l = \sum_k w_{k,l} q_k . \quad (A.3)$$

The tanh function in the hidden layers provides the nonlinear capability of the network. Other nonlinear functions are possible; the sigmoidal function $(1/(1 - \exp[-\sum wx]))$ is used here. Both functions map an infinite possible input range onto a finite output range, -1 to $+1$ in the case of tanh. This imitates the transfer function of neurons.

REFERENCES

Atlas of Low Resolution IRAS Spectra. 1986. IRAS Science Team, prepared by F. M. Olmon & E. Raimond (A&AS, 65, 607)(Atlas)

- Bailer-Jones, C.A.L., Gupta, R. and Singh, H.P. in “Automated Data Analysis in Astronomy”, Eds., Gupta, R., Singh, H.P. and Bailer-Jones, C.A.L., Narosa Publishing House, N. Delhi (2002) pp. 51
- Gulati, R. K., Gupta, R., Gothoskar, P. & Khobragade, S., 1994a, *ApJ*, 426, 340
- Gulati, R. K., Gupta, R., Gothoskar, P. & Khobragade, S., 1994b, *Vistas in Astronomy*, 38(3), 293
- Gulati, R. K., Gupta, R., & Rao, N. K. 1997a, *A&A*, 322, 933
- Gulati, R. K., Gupta, R., & Singh, H. P., 1997b, *PASP*, 109, 843
- Gupta, R., Gulati, R. K., & Singh, H. P., 2001, in Proc. 11th Cambridge Workshop “Cool Star, Stellar Systems, and the Sun – Challenges for the New Millennium”. Eds. R. J. Garcia-Lopez, R. Rebelo, & M. R. Zapatero Osorio, ASP Conf. Ser., 223, CDROM p. 791
- Kwok, S., Volk, K., & Bidelman, W. P., 1997, *ApJ*, 112, 557
- Lahav, O., Storrie-Lombardi, M. C. 1994, *Vistas in Astronomy*, 38 (Special issue on Neural Networks in Astronomy)
- Singh, H. P., Gulati, R. K., & Gupta, R., 1998, *MNRAS*, 295, 312
- Volk, K. & Cohen, M. 1989a, *AJ*, 98, 931
- Volk, K. & Cohen, M. 1989b, *AJ*, 98, 1563
- Volk, K., Kwok, S., Stencel, R. E., Brugel, E., 1991, *ApJS*, 77, 607
- Volk, K., Kwok, S., & Langill, P. P., 1992, *ApJ*, 391, 285
- Volk, K., Kwok, S., & Woodsworth, A. W. 1993, *ApJ*, 402, 292
- von Helden, G., Tielens, A. G. G. M., van Heijnsbergen, D., Duncan, M. A., Hony, S., Waters, L. B. F. M., Meijer, G. 2000, *Science*, 288, 313

Table 1: A short description of the 17 ANN training classes

Source type	Description	ANN Class
Stellar	Stellar photospheric spectra; B-type to early M-type	2
	Lower temp. stellar continuum spectra with no features: mid to late M-type, little circumstellar dust	3
Carbon stars	Strong 11.3 μm emission	1
	Lower temp. continuum ($\sim 250^\circ\text{K}$), e.g., AFGL 3068 & no strong features	10
	Weaker 11.3 μm emission	15
Oxygen-rich AGB stars	Silicate absorption on an intermediate temp. continuum (400 – 200°K)	5
	Stronger 10 μm emission on a higher temp. continuum ($\geq 600^\circ\text{K}$)	6
	Weaker 10 μm emission on a higher temp. continuum ($\geq 600^\circ\text{K}$)	12
	10 μm features in transition from emission to absorption	13
Planetary nebulae (PN) & post-AGB sources (PPN)	Emission lines (PN)	0
	Silicate emission on a low temp. continuum (oxygen-rich PN & PPN)	8
	Lower temp. ($\sim 150^\circ\text{K}$) featureless (carbon-rich PN and PPN)	11
	21 μm emission feature (carbon-rich PPN)	14
ISM spectra: mostly HII regions; includes a few PN, PPN, & galaxies	UIR or PAH features on a flat continuum (HII regions, galaxies, a few PN & PPN)	4
	Low temp. continuum ($\leq 100^\circ\text{K}$) without strong features	7
	10 μm absorption on a low temp. continuum ($\leq 100^\circ\text{K}$), includes a few PPN	9
	UIR or PAH features on a low temp. continuum ($\leq 100^\circ\text{K}$), includes a few PN	16

Table 3. List of LRS sources misclassified by ANN

IRAS designation	Catalog class	ANN class	IRAS designation	Catalog class	ANN class	IRAS designation	Catalog class	ANN class
04395+3601	0	13	15380–6545	3	12	14198–6115	4	5
17069–4149	0	7	17282–5102	3	2	14206–6151	4	16
21014–1133	0	8	17504–0234	3	2	15246–5612	4	16
22036+5306	0	16	19369+2823	3	1	15535–5328	4	5
03293+6038	1	15	20056+1834	3	13	16041–4912	4	5
04340+4623	1	13	22476+4047	3	2	16204–4717	4	5
05405+3240	1	15	23092+5236	3	15	16225–4844	4	14
08011–3627	1	6	23095+5925	3	2	16331–4637	4	16
08086–3905	1	13	00450–2533	4	16	16467–4255	4	13
08534–5055	1	13	01056+6251	4	5	16573–4619	4	5
08544–4431	1	13	02401–0013	4	10	17076–4702	4	13
10098–5742	1	14	04064+5052	4	13	17324–3152	4	16
12195–6830	1	13	05044–0325	4	5	17355–3241	4	2
13045–6404	1	13	05345+3157	4	5	17486–2345	4	5
13064–6433	1	13	06114+1745	4	16	18077–2614	4	5
15084–5702	1	13	06319–0501	4	5	18092–1742	4	9
15261–5702	1	15	07013–1128	4	13	18162–0246	4	13
15469–5311	1	4	07017–1114	4	5	18162–1612	4	16
16093–4808	1	15	08247–4223	4	5	18254–1149	4	5
16192–4900	1	15	08438–4340	4	9	18310–2834	4	5
16455–4349	1	4	09014–4736	4	13	18312–1209	4	5
17199–3512	1	4	10105–5719	4	16	18320–0352	4	15
17289–3106	1	13	10267–5658	4	13	18357–0604	4	5
18301–0656	1	6	10366–5931	4	13	18463–0052	4	16
18367–0452	1	13	11356–6144	4	13	19097+0847	4	16
18551+0323	1	15	11418–6706	4	13	19156–0935	4	15
21223+5114	1	13	12421–6217	4	15	19193+1504	4	5
16063–4906	2	3	13065–6354	4	5	19343+2026	4	5
00192–2020	3	2	14092–6506	4	5	21282+5050	4	14
21345+5410	4	15	05390+1448	6	12	19039+0809	6	12

Table 3—Continued

IRAS designation	Catalog class	ANN class	IRAS designation	Catalog class	ANN class	IRAS designation	Catalog class	ANN class
22308+5812	4	16	06434–3628	6	12	19089+1542	6	8
23541+7031	4	5	06546–2353	6	12	19231–2717	6	13
09199–5447	5	14	08189+0507	6	12	19291+2012	6	10
17317–3331	5	16	10174–5704	6	8	19354+5005	6	12
17443–2949	5	16	10360–5633	6	12	19420+3318	6	10
18168–1520	5	13	11113–5949	6	12	20004+2955	6	8
18257–1000	5	16	11492–6052	6	12	20273+3932	6	1
18316–0746	5	16	12188–6246	6	10	20526–5431	6	12
18407–0619	5	4	12230–5943	6	12	21044–1637	6	12
18491–0207	5	16	14297–6010	6	10	21389+5405	6	12
19065+0832	5	16	16235+1900	6	12	21419+5832	6	12
19352+2030	5	9	16275–2638	6	13	22000+5643	6	12
20110+3321	5	9	16316–5026	6	12	22196–4612	6	12
20187+4111	5	4	16367–2046	6	12	22480+6002	6	8
20318+3829	5	4	16434–4545	6	10	23416+6130	6	8
20547+0247	5	4	17189–6501	6	10	05305+3029	7	16
23151+5912	5	16	17237–3102	6	12	09032–3953	7	11
00001+4826	6	12	17269–2625	6	12	11143–6113	7	0
01010+7434	6	12	17450–2724	6	10	14394–6004	7	9
01251+1626	6	12	17515–2407	6	13	16268–4556	7	0
01597+5459	6	12	17538–3728	6	12	16342–3814	7	9
02360+5922	6	12	18038–1614	6	13	17078–3927	7	0
03489–0131	6	12	18207–1029	6	10	20028+3910	7	11
03503+6925	6	12	18243+0352	6	12	21078+5211	8	0
04137+3114	6	12	18303–0519	6	13	06053–0622	9	7
04188+2819	6	8	18309–6955	6	12	07399–1435	9	7
04292+3100	6	12	18363–0523	6	8	10019–5712	9	5
04525+3028	6	8	18518+0358	6	10	10460–5811	9	7
13416–6243	9	14	07418–2850	12	6	18586–1249	12	3
16313–4840	9	14	07434–3750	12	6	19055+0613	12	3

Table 3—Continued

IRAS designation	Catalog class	ANN class	IRAS designation	Catalog class	ANN class	IRAS designation	Catalog class	ANN class
18032–2032	9	16	09411–5933	12	1	19111+2555	12	1
18100–1915	9	5	09508–4345	12	6	19328+3039	12	6
18316–0602	9	16	09564–5837	12	3	19510–5919	12	3
18317–0757	9	7	10383–7741	12	3	19585+5200	12	3
18379–0500	9	5	11202–5305	12	13	20111–4708	12	3
18566+0408	9	16	13248–7851	12	3	20416+1903	12	3
19310+1745	9	14	13548–3049	12	1	20438–0415	12	1
19566+3423	9	14	14129–5940	12	6	20507+2310	12	6
02152+2822	10	1	14234–5359	12	3	23212+3927	12	1
06505–0450	10	13	15410–0133	12	6	05073+5248	13	6
13522–5619	10	13	15492+4837	12	3	06259–1301	13	6
14318–5937	10	6	16052–2339	12	3	06308+0402	13	5
16279–4709	10	13	16306+7223	12	3	06364+0846	13	8
17056–3959	10	6	16328–4656	12	1	06491–0654	13	6
05573+3156	11	14	16334–3107	12	3	07180–1314	13	6
09370–4826	11	14	16383–1952	12	6	07376–2827	13	6
13308–6209	11	0	16387–2700	12	3	08357–1013	13	6
19500–1709	11	14	16438–1133	12	6	09354–5627	13	10
00007+5524	12	6	16494–1252	12	6	10028–5825	13	8
00245–0652	12	6	16534–3030	12	3	10077–5304	13	6
01150+5732	12	3	17201–4613	12	3	10277–5730	13	4
03082+1436	12	3	17297+1747	12	3	10287–5733	13	6
05132+5331	12	6	17318–2342	12	6	10323–4611	13	6
05450–3142	12	6	17505–7021	12	3	10481–6930	13	6
06210+4918	12	3	17578–1700	12	3	11214–6448	13	6
06261+1637	12	3	18347–0241	12	3	11296–4431	13	6
07091–2902	12	3	18378–3731	12	3	11467–6234	13	6
11528–5902	13	6	16320–4419	13	10	18061–1743	13	6
11575–7754	13	6	16335–4707	13	6	18083–2630	13	6
12043–6225	13	6	16350–4754	13	6	18085–1832	13	6

Table 3—Continued

IRAS designation	Catalog class	ANN class	IRAS designation	Catalog class	ANN class	IRAS designation	Catalog class	ANN class
12222–4652	13	6	16365–4717	13	6	18089–2952	13	3
12384–4536	13	6	16399–3548	13	10	18222–1544A	13	6
13243–6159	13	6	16409–5128	13	6	18373–0021	13	6
13366–6222	13	6	16414–4941	13	6	18373–0922	13	6
13517–6515	13	6	16490–4618	13	6	18381+0020	13	6
13527–6117	13	10	16538–4135	13	6	18409+0431	13	6
14273–6153	13	6	16567–4659	13	6	18471–0259	13	6
14591–4438	13	6	16580–4424	13	6	18530+0817	13	6
15008–5808	13	6	16598–4117	13	6	18588–1915	13	6
15044–5822	13	6	17030–4246	13	10	19007–3826	13	6
15054–5458	13	10	17109–3243	13	6	19043+1009	13	6
15152–6241	13	6	17132–5003	13	6	19135+0931	13	6
15163–5525	13	8	17186–4208	13	6	19171+1119	13	5
15174–4821	13	6	17239–2812	13	6	19229+1708	13	6
15236–5556	13	6	17362–3322	13	6	19244+1809	13	6
15408–5413	13	4	17368–3000	13	6	19493+2905	13	10
15500–5135	13	6	17382–1704	13	6	19520+2759	13	4
15527–6041	13	6	17401–5730	13	6	20095+2726	13	6
15532–4802	13	6	17479–2927	13	6	20171+3519	13	5
16031–4856	13	6	17507–1122	13	6	20217+3330	13	6
16038–5008	13	6	17559–2848	13	6	20267+2105	13	6
16055–4621	13	5	18006–3213	13	6	20365+1154	13	6
16061–4555	13	10	18022–1432	13	6	20509+4212	13	6
16077–5830	13	6	18027–2314	13	6	21453+5959	13	6
16109–4651	13	6	18046–2322	13	6	22525+6033	13	6
16146–5257	13	6	18050–0518	13	6	16235–4832	14	10
03112–5730	15	1	10329–3918	15	2	18400–0704	15	13
05418–3224	15	1	12226+0102	15	1	18551+1345	15	4
05426+2040	15	1	12544+6615	15	2	19314–1629	15	1
05440+4311	15	1	13136–4426	15	1	19537+2212	15	1

Table 3—Continued

IRAS designation	Catalog class	ANN class	IRAS designation	Catalog class	ANN class	IRAS designation	Catalog class	ANN class
06183+1135	15	1	14232–6106	15	14	20014+2830	15	13
06230–0930	15	1	15193–5656	15	4	15357–5239	16	5
07098–2012	15	1	16296–4417	15	13	20068+3328	16	7
07538–3928	15	3	17044–3722	15	1	20286+4105	16	14
08304–4313	15	14	17047–2848	15	1	21334+5039	16	7
08439–2734	15	1	17048–1601	15	1	22566+5830	16	0
09521–7508	15	1	17544–2951	15	1			
10239–5818	15	4	18234–2206	15	1			

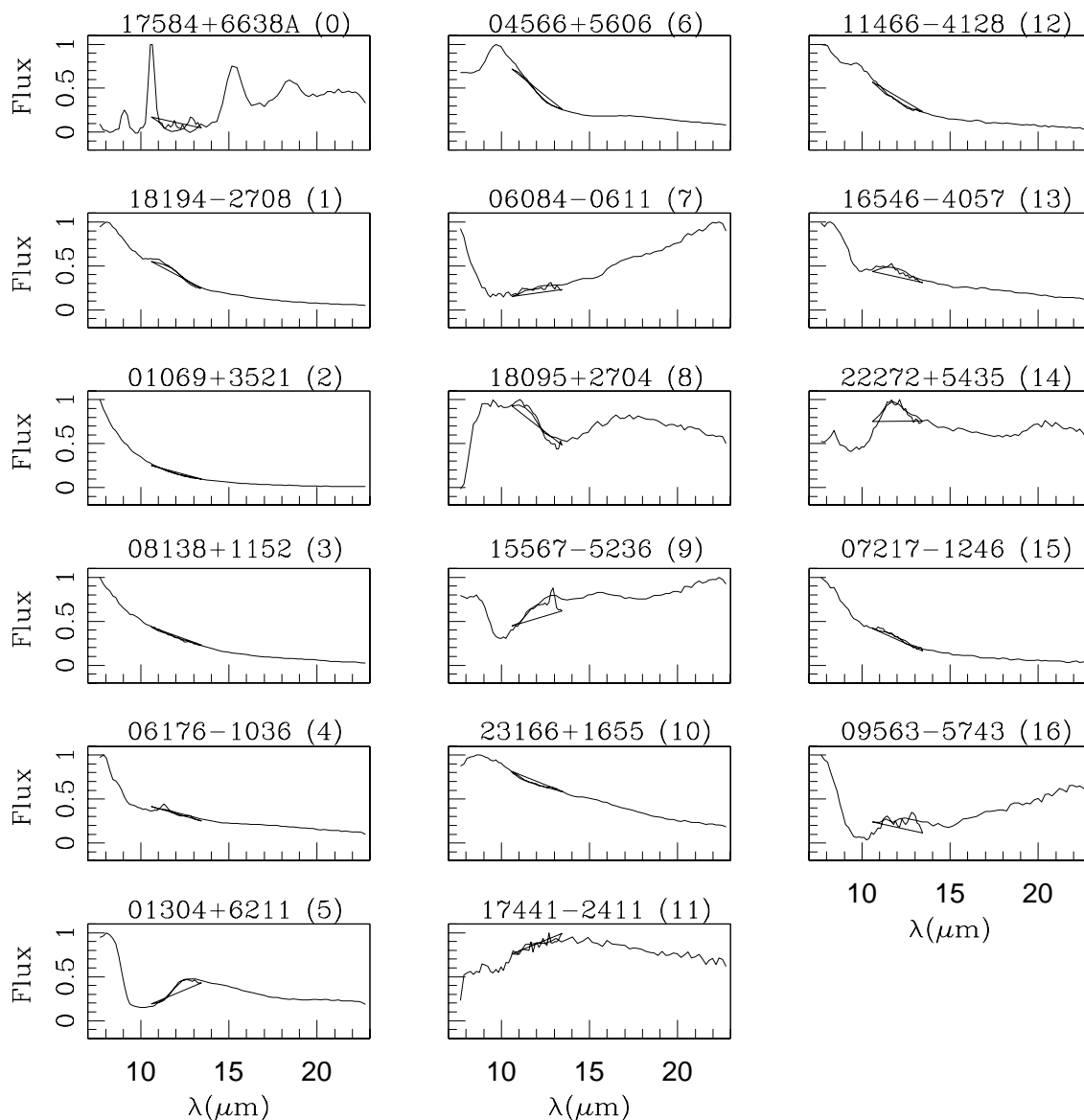


Fig. 1.— The LRS spectra for the 17 training classes. There are ten training spectra each for the 17 Catalog classes but only one representative spectrum is shown. For each spectrum the IRAS name and the Catalog class (in parenthesis) are given above the plot. Please note that there exists a crossover region between the "blue" and the "red" spectra (due to the instrument's settings) ranging between the 10-14 μm and this is seen in these plots.

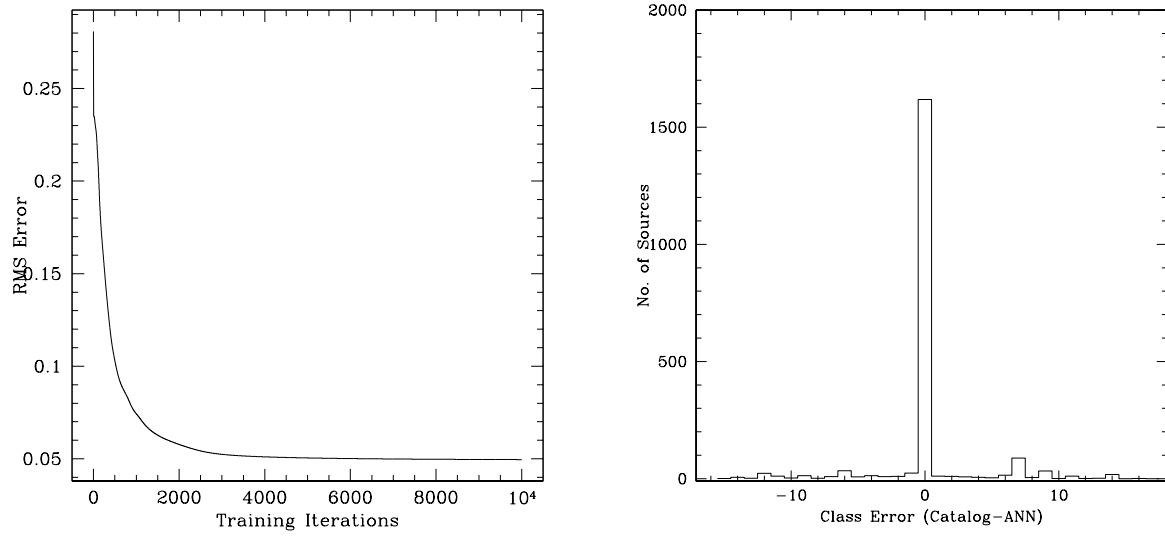


Fig. 2.— ANN learning curve for 10000 iterations (left panel). The RMS error refers to the RMS difference between the computed output and the desired output for each iteration. The right panel shows the histogram of classification accuracy for the 2000 test patterns with 17 training classes.

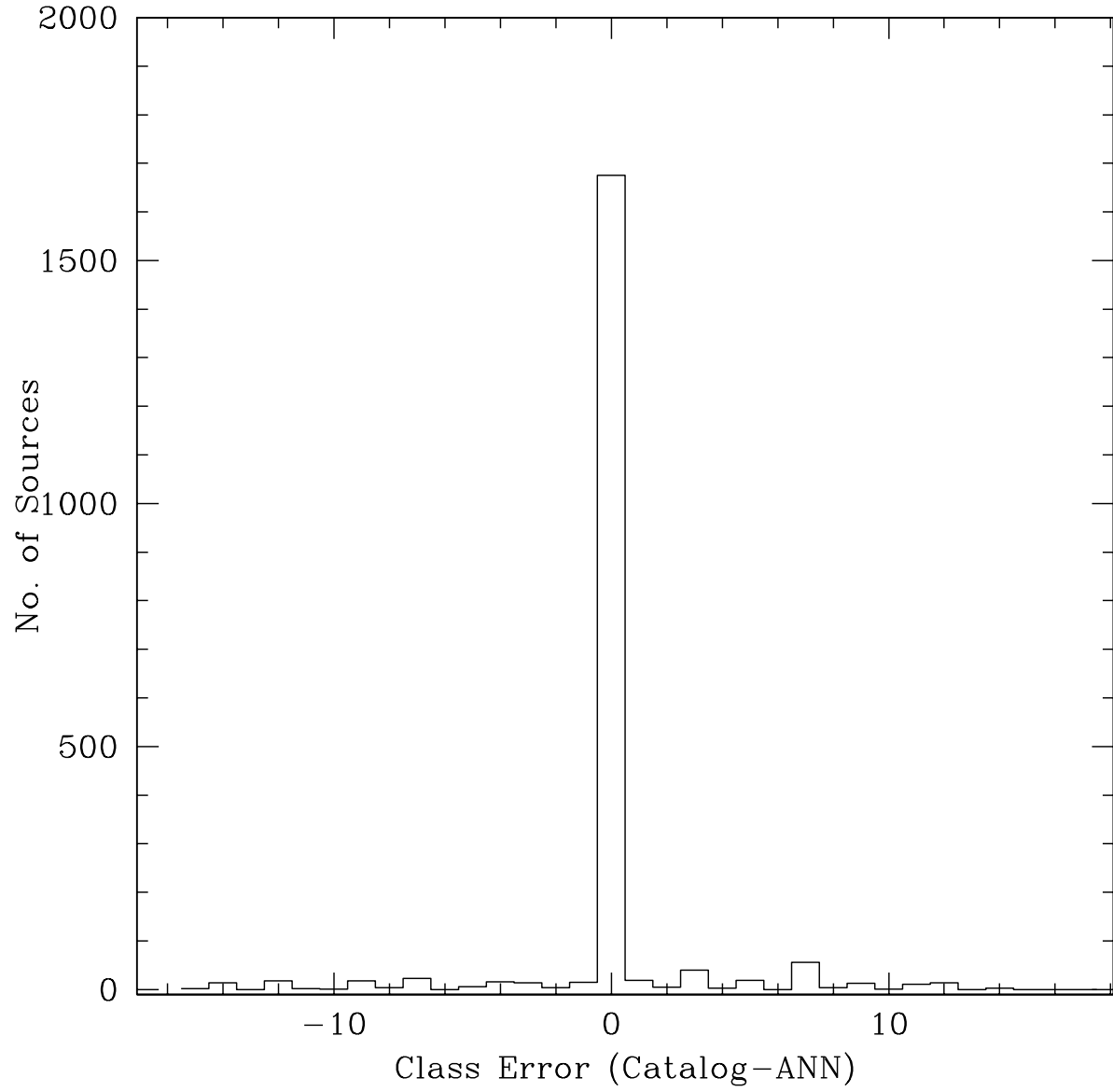


Fig. 3.— The histogram of classification accuracy for the 2000 test patterns with 16 training classes (class 12 trained as class 6)

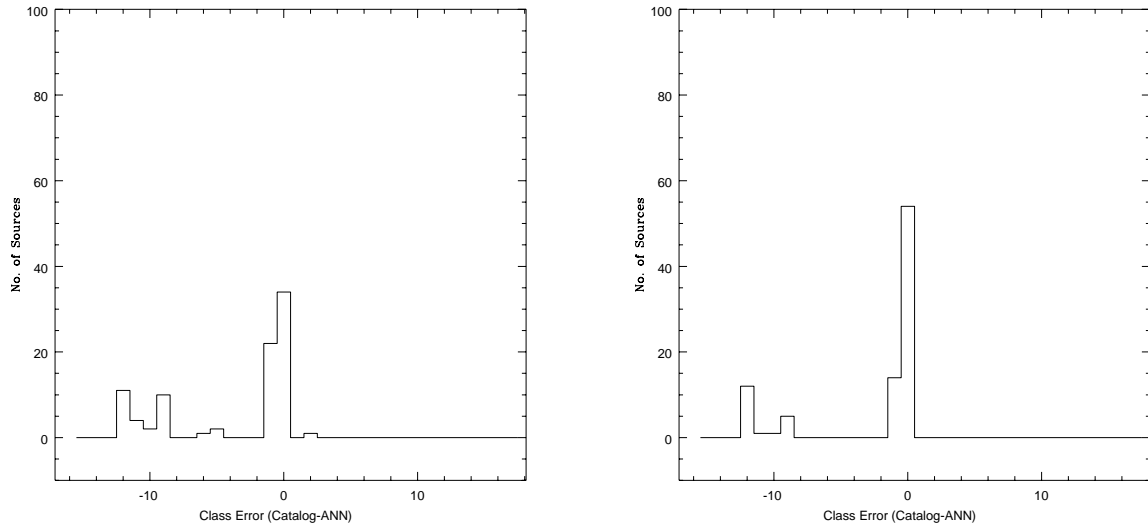


Fig. 4.— Histogram of classification accuracy for the 87 test patterns of class 4 with 17 training classes (left panel) and with combined training class 6 and class 12 (right panel)

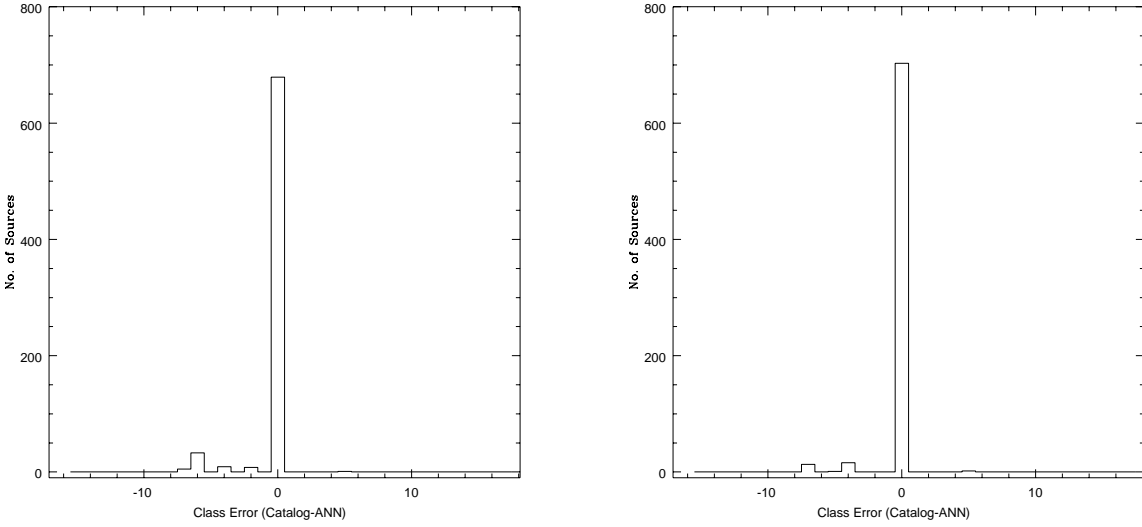


Fig. 5.— Histogram of classification accuracy for the 735 test patterns of class 6 with 17 training classes (left panel) and with combined training class 6 and class 12 (right panel)

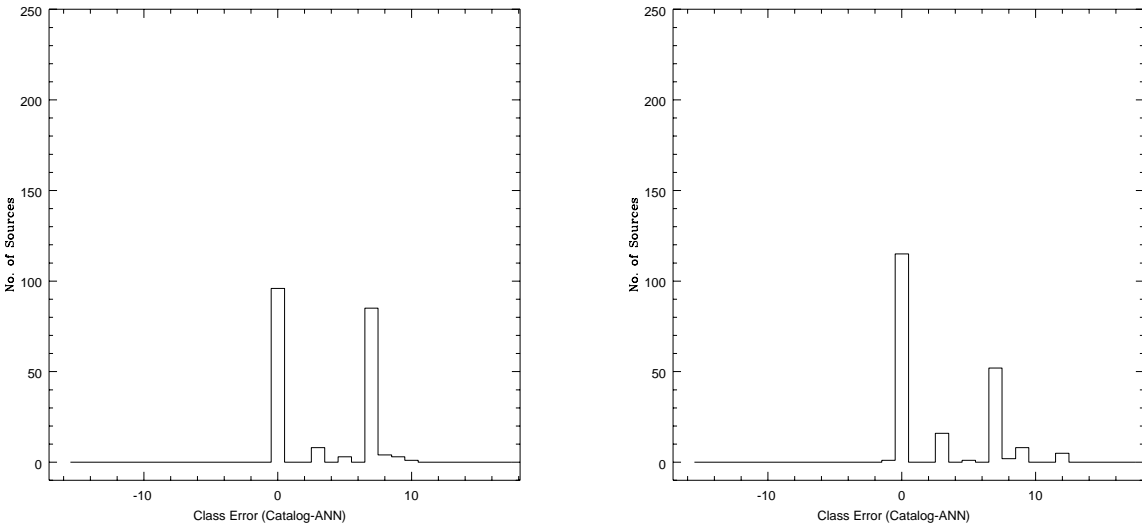


Fig. 6.— Histogram of classification accuracy for the 200 test patterns of class 13 with 17 training classes (left panel) and with combined training class 6 and class 12 (right panel)

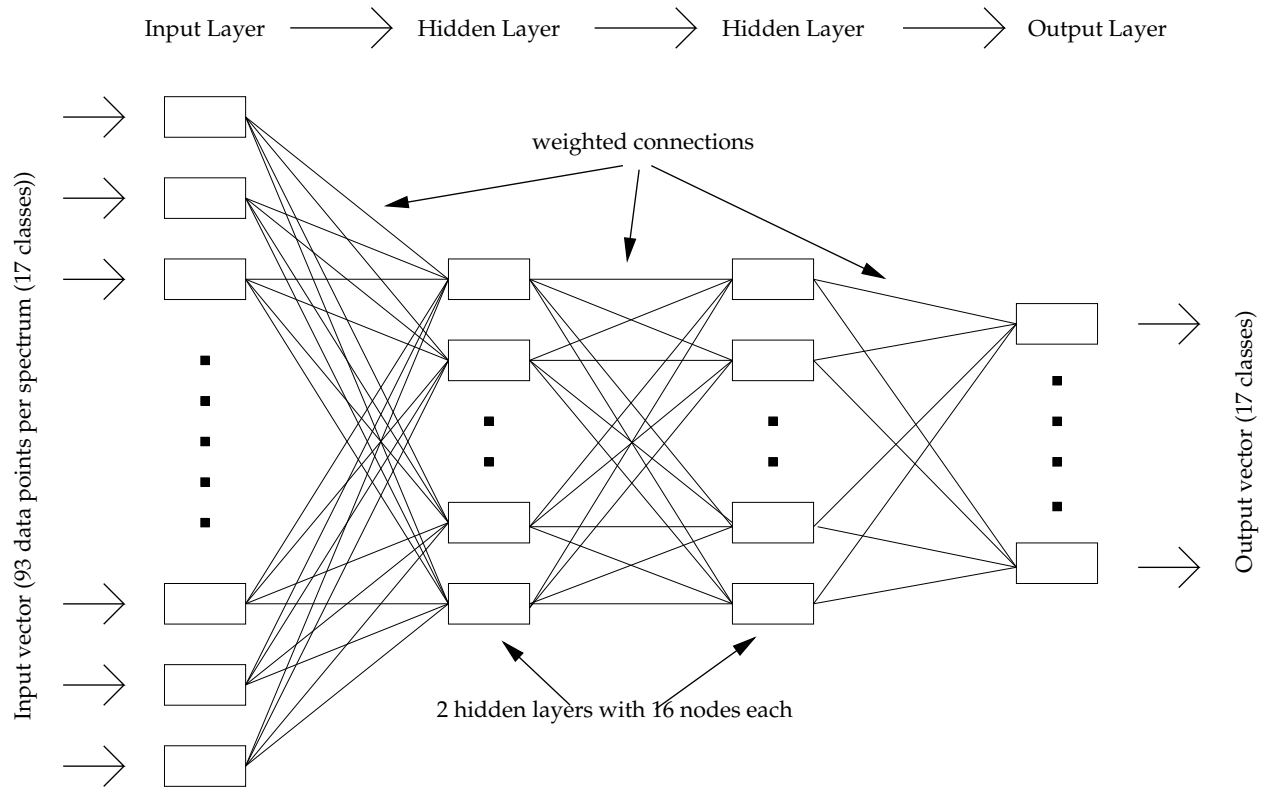


Fig. 7.— Feedforward artificial neural network architecture for the problem under investigation